Steel and Composite Structures, *Vol. 17, No. 6 (2014) 891-906*
DOI: http://dx.doi.org/10.12989/scs.2014.17.6.891

Wave propagation in a concrete filled steel tubular column due to transient impact load

Xuanming Ding [*1], Yuming Fan [2a], Gangqiang Kong [2b] and Changjie Zheng [2c]

[1] *Key Laboratory of New Technology for Construction of Cities in Mountain Area, Chongqing University, Chongqing 400045, China*
[2] *Key Laboratory of Ministry of Education for Geomechanics and Embankment Engineering, Geotechnical Research Institute, Hohai University, 1 Xikang Road, Nanjing 210098, China*

(*Received October 13, 2013, Revised July 16, 2014, Accepted October 02, 2014*)

Abstract. This study aims to present a three dimensional finite element model to investigate the wave propagation in a concrete filled steel tubular column (CFSC) due to transient impact load. Both the concrete and steel are regarded as linear elastic material. The impact load is simulated by a semi sinusoidal impulse. Besides the CFSC models, a concrete column (CC) model is established for comparing under the same loading condition. The propagation characteristics of the transient waves in CFSC are analyzed in detail. The results show that at the intial stage of the wave propagation, the velocity waves in CFSC are almost the same as those in CC before they arrive at the steel tube. When the waves reach the column side, the velocity responses of CFSC are different from those of CC and the difference is more and more obvious as the waves travel down along the column shaft. The travel distance of the wave front in CFSC is farther than that in CC at the same time. For different wave speeds in steel and concrete material, the wave front in CFSC presents an arch shape, the apex of which locates at the center of the column. Differently, the wave front in CC presents a plane surface. Three dimensional effects on top of CFSC are obvious, therefore, the peak value and arrival time of incident wave crests have great difference at different locations in the radial direction. High-frequency waves on the waveforms are observed. The time difference between incident and reflected wave peaks decreases significantly with r/R when $r/R < 0.6$, however, it almost keeps constant when $r/R \geq 0.6$. The time duration between incident and reflected waves calculated by 3D FEM is approximately equal to that calculated by 1D wave theory when r/R is about 2/3.

Keywords: wave propagation; concrete filled steel tubular column; transient impact load; finite element method; three dimensional effects

1. Introduction

Concrete filled steel tubular columns (CFSC) are used extensively in the construction, offshore, mining and security industries (Bambach *et al*. 2008). They have several benefits such as high

*Corresponding author, Ph.D., Professor, E-mail: dxmhhu@163.com
[a] Master Student, E-mail: geofym@163.com
[b] Ph.D., E-mail: gqkong1@163.com
[c] Ph.D., E-mail: zhengchj1989@163.com

Copyright © 2014 Techno-Press, Ltd.
http://www.techno-press.org/?journal=scs&subpage=8 ISSN: 1229-9367 (Print), 1598-6233 (Online)

load-bearing capacity, inherent ductility and toughness, etc. (Bambach *et al*. 2008, Na and Kundu 2002, Chung *et al*. 2013). Therefore, they are efficient members in structural applications including bridges, tall buildings and piled foundations (Wheeler and Bridge 2004).

CFSC may be subjected to many kinds of loads, i.e., the static and dynamic loads. Because CFSC is made of steel and concrete, the mechanical behavior of these structures is different from the steel tube (ST) and concrete column (CC), which have attracted the attentions of many researchers in engineering. The mechanical behaviors of CFSC under static loading were experimentally and numerically studied by Jai Woo Park and Sung Mo Choi (2013), Chen and Zhang (2012), Alifujiang Xiamuxi and Akira Hasegawa (2012), O'Shea and Bridge (2000). The structural behaviors of CFSC subjected to flexural loading were also investigated by experimental and analytical methods (Chung *et al*. 2013, Wheeler and Bridge 2006).

Many researches on mechanical behaviors of CFSC under cyclic and dynamic loading were also reported in literatures (Usami *et al*. 1997, Gajalakshmi and Helena 2012, Susantha *et al*. 2002). The seismic performance of reinforced concrete-filled steel tube (RCFST) pile bridge bents were studied, the strain limit states were proposed and the expressions to relate the strain limits with section curvatures were developed (Montejo *et al*. 2012). The influences of the filled-in concrete on the strength, ductility and energy absorption capacity of the column under a constant compressive axial load and cyclic lateral loads were studied by experimental method (Ge and Usami 1996). In addition, the dynamic behavior of CFSC under impact loading were researched by numerical, experimental and analytical methods (Shan *et al*. 2007, Huo 2009, Bambach *et al*. 2008).

For a steel tube filled with concrete, the construction quality of the concrete is of great importance. Non-destructive methods (i.e., pulse-echo methods) are extensively adopted to detect the integrity of concrete structures. Pulse-echo methods (i.e., radar, impact-echo and ultrasonic impulse-echo) were applied for testing concrete speciments with metal ducts (Krause *et al*. 1997). The interface inspection of concrete-filled steel pipes was checked by guided wave techniques (Na and Kundu 2002). The drivability of filled FRP tubes and prestressed concrete piles with the same cross-sectional area and concrete strength was analyzed by using Program Microwave (Mirmiran *et al*. 2002). The three dimensional effects of large-diameter concrete piles in low strain testing werestudied by finite element method (Chow *et al*. 2003) and analytical method (Ding *et al*. 2011a, b and c). Ye *et al*. (2005) researched the effect of pile length on velocity responses of concrete filled steel pile (CFSP) and proposed a method to calculate the pile length in low strain integrity testing.

As far as the authors are aware, however, wave propagations in CFSC under transient point load are still unknown. The purpose of this paper is to reveal the wave propagation characteristics in CFST for integrity testing by non-destructive methods (i.e., pulse-echo methods). Therefore, a three dimensional finite element model of CFST subjected to transient impact load is established to investigate the wave propagation characteristics.

2. Computational model and parameters

The finite element package ABAQUS is used to simulate the wave propagation in CFSC due to transient impact load. The computational model of CFSC is shown as Fig. 1, where R is the radius of the CFSC and d is the wall thickness of the steel tube.

An impact load applies at the center of the column top. The impact load is simulated by a semi sinusoidal impulse, which can be expressed by the following equation

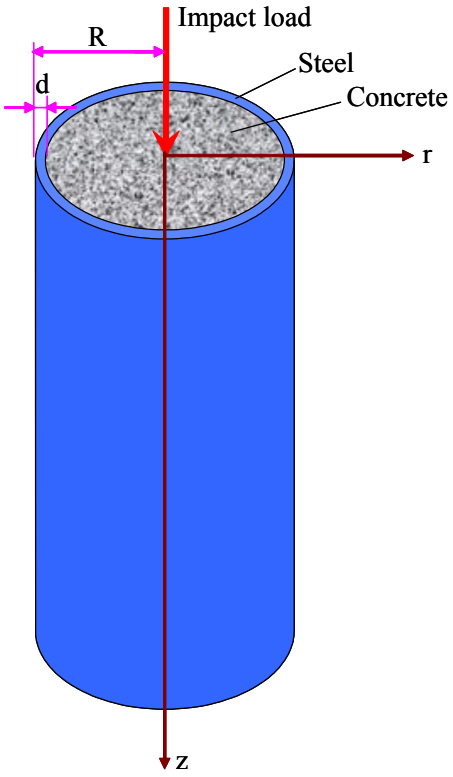

Fig. 1 Computational model of CFSC

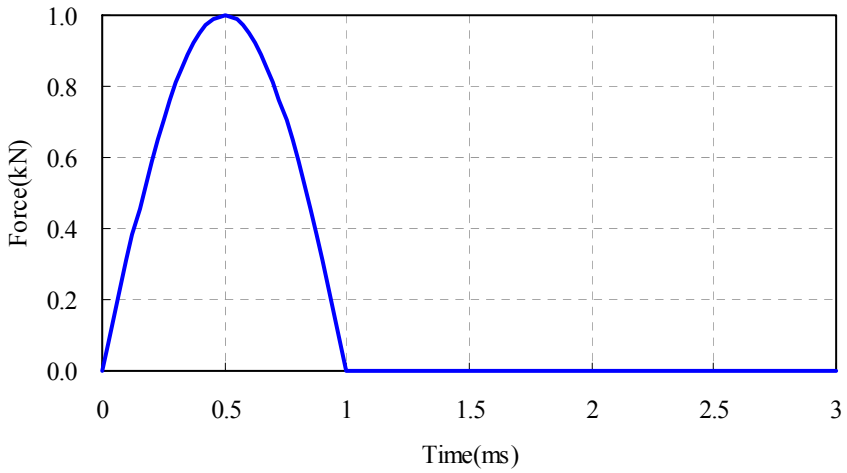

Fig. 2 The impact load time history

$$p(t)=\begin{cases} p_0 \sin(\pi t / T_d) & 0 \le t \le T_d \\ 0 & t > T_d \end{cases} \tag{1}$$

Table 1 The parameters of the CFSC

Material	E_s, E_c (GPa)	ρ_s, ρ_c (kg/m^3)	v_s, v_c
Steel	210	7850	0.3
Concrete	30	2500	0.2

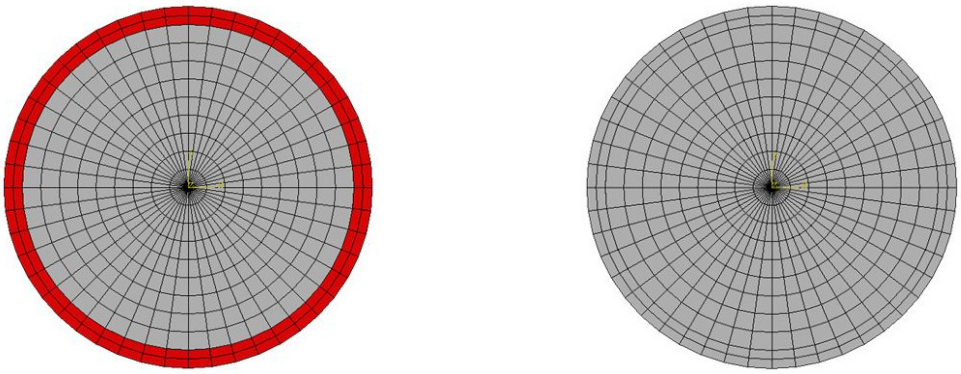

(a) CFSC (b) CC

Fig. 3 Top view of the FEM meshes

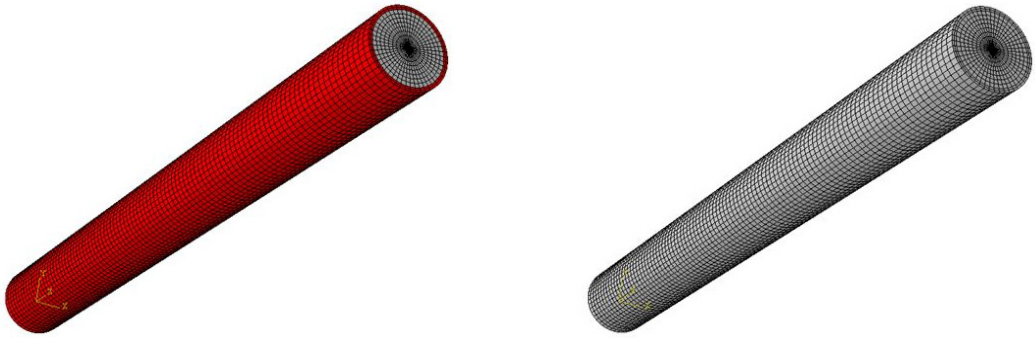

(a) CFSC (b) CC

Fig. 4 3D FEM meshes

where p_0 and T_d are peak value and duration time of the impulse force, respectively. In this study p_0 = 1 kN and T_d = 1 ms. The impact load time history is shown as Fig. 2.

Both the concrete and steel are regarded as linear elastic material. The interface between steel and concrete is contact perfectly. The parameters adopted in this paper are shown in Table 1, where E_s and E_c are the elastic modulus of the steel and concrete, respectively; ρ_s and ρ_c are the density of the steel and concrete, respectively; v_s and v_c are Poisson's ratio of the steel and concrete, respectively.

The concrete and steel mediums are discretized into three-dimensional finite elements with eight nodes .The FEM meshes of CFSC are shown in Figs. 3(a) and 4(a). To analyze the propagation characteristics of the transient waves, CC and steel column (SC) models are also

Table 2 The calculation cases

Case	Model	R (m)	d (m)	E_c (GPa)	T_d (ms)	d/R
1	CFSC	0.75	0.075	30	1	0.10
2	CFSC	0.50	0.05	30	1	0.10
3	CFSC	0.25	0.025	30	1	0.10
4	CFSC	0.25	0.025	21	1	0.10
5	CFSC	0.25	0.025	15	1	0.10
6	CC	0.25	0	30	1	0.00
7	CFSC	0.25	0.005	30	1	0.02
8	CFSC	0.25	0.0625	30	1	0.25
9	CFSC	0.25	0.125	30	1	0.50
10	CFSC	0.25	0.1875	30	1	0.75
11	SC	0.25	0.25	30	1	1.00

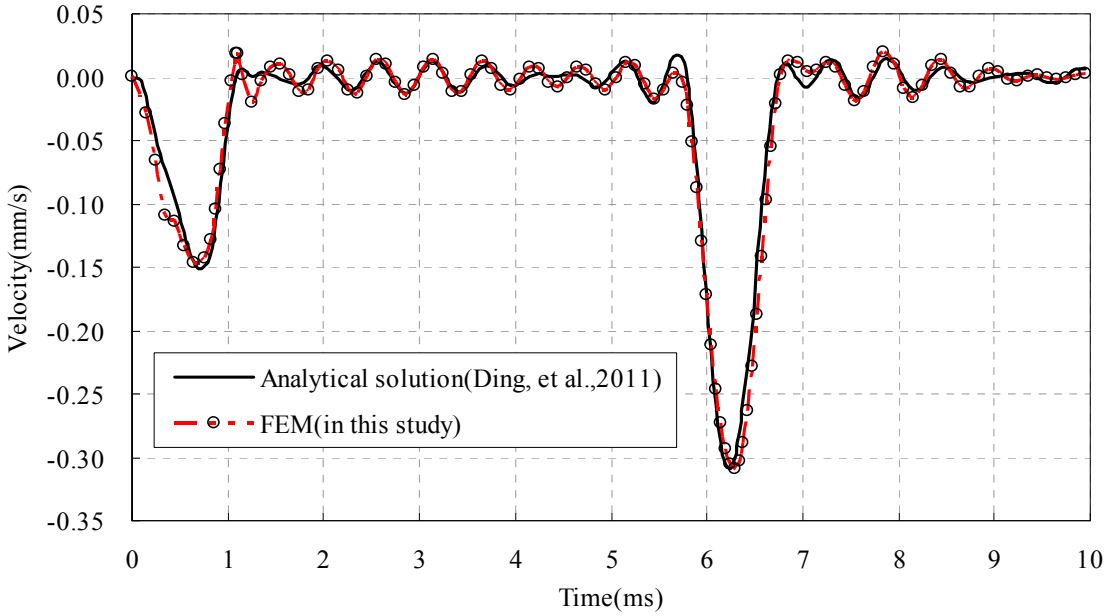

Fig. 5 Comparison of velocity responses calculated by analytical solution with FEM at $r = 0.60R$ (Case 6)

established for comparing under the same loading in this study. The calculation cases are shown in Table 2. The column lengths of all cases are 10 m.

3. Verification of the numerical model

Ding *et al*. (2011c) derived an analytical solution of 3D wave equation for a larger-daimeter pile subjected to a transient point loading. The FEM model of Case 6 is a concrete pile model, thus

the numerical results of Case 6 in this study are compared with the results calculated by the analytical solution proposed by Ding *et al*. (2011c), as shown in Fig. 5. The comparison results indicate that the arrival time and peak value of the incident and reflected waves in this study match well with those of Ding *et al*. (2011c).

4. Propagation characteristics of the transient waves

When the transient point load applies at the center of the column top, the generated stress waves propagate not only in the axial direction but also in the radial direction. As a result, the velocity responses vary with r and z simultaneously during the wave propagation.

Fig. 6 shows snapshots of velocity waves in CFSC of Cases 1 to 3 with different radius at t = 1 ms. Because d/R is the same for these cases, the steel ratios (i.e., the ratio of area of steel section to area of gross section) are the same, namely the average wave speed are the same. As a result, the travel distances of the wave fronts for these columns with different radius are almost the same. Fig. 6 reveals that all the wave fronts are in the depth of about 3.9 m.

For different wave speeds in steel and concrete, the wave front in steel tube is different from that in concrete. The wave fronts marked in Fig. 6 are locally enlarged and represent in Fig. 7. Fig. 7 shows that the velocity waves in steel propagate faster than those in concrete, as a result, the wave fronts in CFSC present an arch shape, the apex of which locates at the center of the column. The larger the radius, the higher the arch height.

Fig. 8 shows the snapshots of the velocity waves in CFSC and CC. At the intial stage of the wave propagation, the velocity waves propagate in the concrete from the center to the side of

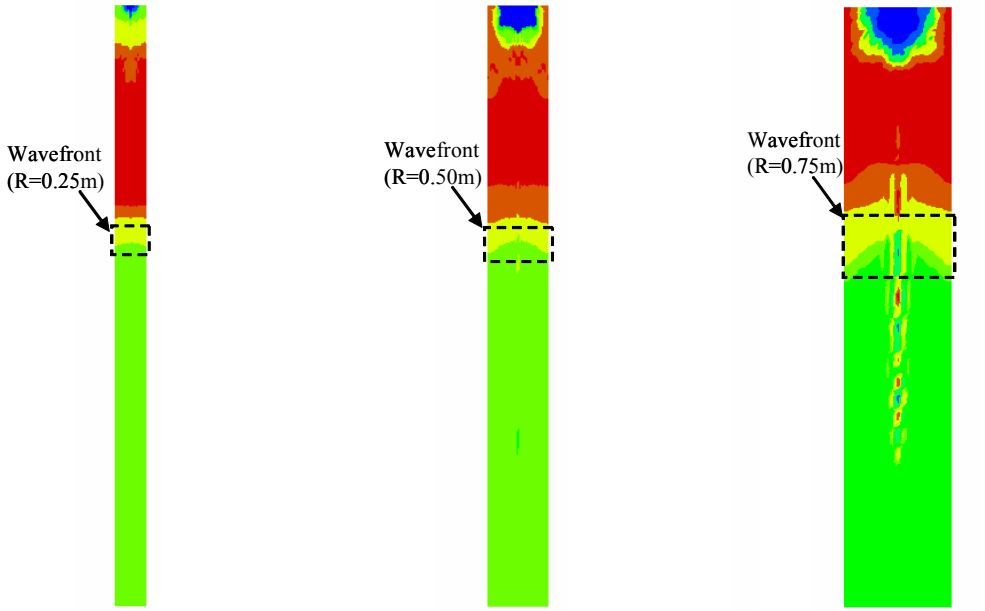

(a) R = 0.25 m (Case 3) (b) R = 0.50 m (Case 2) (c) R = 0.75 m (Case 1)

Fig. 6 Snapshots of velocity waves in CFSC at t = 1 ms

the column, as a result, the snapshots of velocity waves of CFST and CC are almost the same before the waves arrive at the steel tube (as shown in Fig. 8(a)). When the waves reach the column side, the velocity waves of CFST are different from those of CC and the difference is more and more obvious as the waves travel down along the column shaft due to different wave speeds in concrete and steel (as shown in Figs. 8(b) and 8(c)). The wave speed in steel is faster than that in concrete, therefore, the travel distance of wave front in CFSC is farther than that in CC(as shown in Figs. 8(d) and 8(e)). As a result, when the wave front in CFSC arrives at the column tip (z = 10 m), that in CC is still at the depth of about 8.6 m at 2.5 ms (as shown in Fig. 8(f)).

The wave front in CFSC presents a curved surface, therefore, the waves in steel tube reach the column tip much earlier than those in concrete near column center. Differently, the wave front in CC is a plane surface, therefore, the waves near the side and center of the column arrive at the column tip almost at the same time.

As shown in Figs. 8(g) and 8(h), the waves propagate downward along column shaft and then reflect back at the column tip, afterward they propagate upward from the tip to top of the column. The wave front of the reflected waves in CFSC reaches the top of the column at about 4.8 ms, but that in CC is about 5.6 ms.

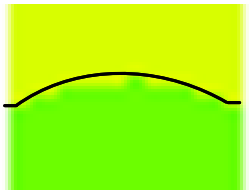

(a) R = 0.25 m (Case 3)

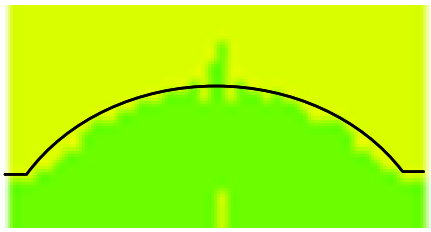

(b) R = 0.50 m (Case 2)

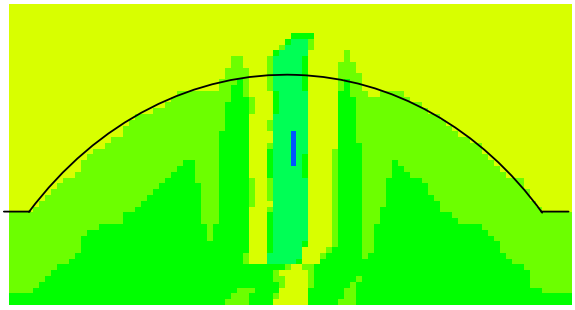

(c) R = 0.75 m (Case 1)

Fig. 7 The wavefronts of velocity waves in CFSC at t = 1 ms

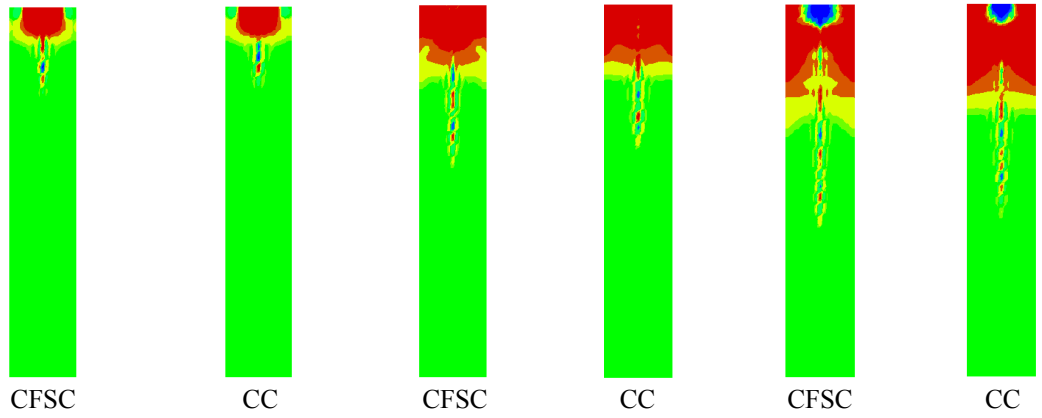

(a) 0.25 ms (b) 0.5 ms (c) 0.75 ms

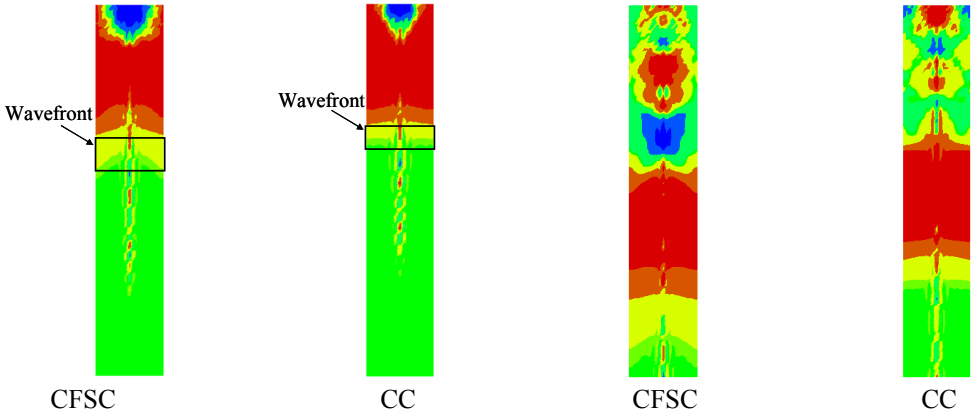

(d) 1 ms (e) 2 ms

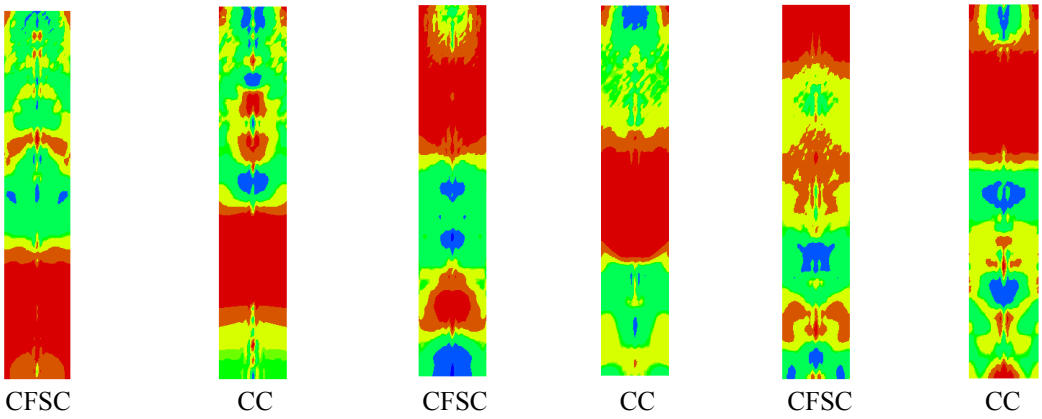

(f) 2.5 ms (g) 4.8 ms (h) 5.6 ms

Fig. 8 Snapshots of velocity waves in CFSC and CC (Case 1)

5. Three dimensional effects of the velocity waves on the columntop

5.1 The velocity responses on the column top

The velocity responses at different locations on the top of CFSC of Case 2 are shown in Fig. 9. The results reveal that three dimensional effects are obvious on the top of CFSC, as a result, the peak value and arrival time of incident wave crests have great difference at different locations in the radial direction. Shorter distance to the column center results in larger peak value and earlier arrival time of incident waves. The reflected waves from the tip of CFSC are also different at different locations. The arrival time of the reflected wave crest at the point on the steel wall (i.e., r/R = 1.0) are earlier than the point far from the steel wall (i.e., r/R = 0.25) because the wave speed in steel is faster than that in concrete. However, the peak values of the reflected waves at different locations are almost the same.

The results in Fig. 9 also show that the velocity response curves are not smooth between the incident and reflected waves. There are high-frequency waves on the waveforms. The peaks and phases of the high-frequency waves are not the same at different locations. The peak values of high-frequency waves corresponding to r/R = 0.50 and 0.75 are smaller than those corresponding to r/R = 0.25 and 1.00. The high-frequency waves corresponding to r/R = 0.25 and 0.50 have opposite phases as those corresponding to r/R = 0.75 and 1.00. Therefore, the high-frequency waves near the center and the side of CFSC have the largest phase difference and peak value.

At the same location, the velocity responses of CFSC and CC are different. The results in Figs.10 and 11 show that the peak value of the incident wave of CFSC is the same as that of CC at the point close to column center (i.e., $r = 0.25R$), however, they are different at the point close to column side (i.e., $r = 0.75R$). The peak value of incident wave of CFSC is smaller than that of CC at the location $r = 0.75R$. This is because the velocity response at the point near the side of CFSC is affected by the reflected waves from the wall of steel tube, which results in the weakening of incident waves. The comparison also reveals that the arrival times of incident waves are almost the

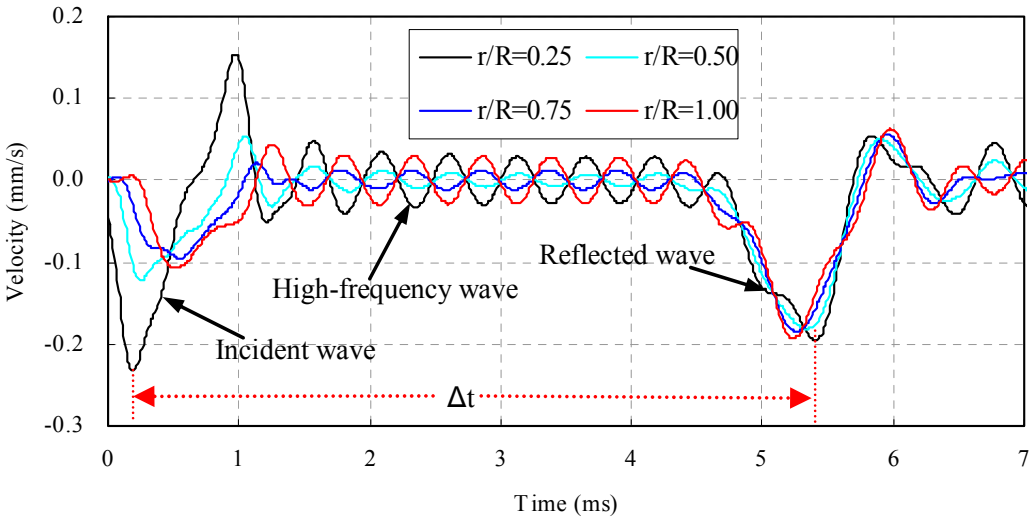

Fig. 9 Velocity responses at different locations on the top of CFSC

same at different points. However, the peak time of reflected wave from the tip of CFSC is earlier than that of CC because of the difference of wave speeds in steel and concrete. The peak value of reflected wave from the tip of CFSC is smaller than that of CC since the density of steel is larger than that of concrete, which causes smaller dynamic response.

5.2 Time difference between incident and reflected wave peaks

Fig. 12 shows effects of d/R on time difference between incident and reflected wave peaks. The time differences between incident and reflected waves at different locations on the top of CFSC

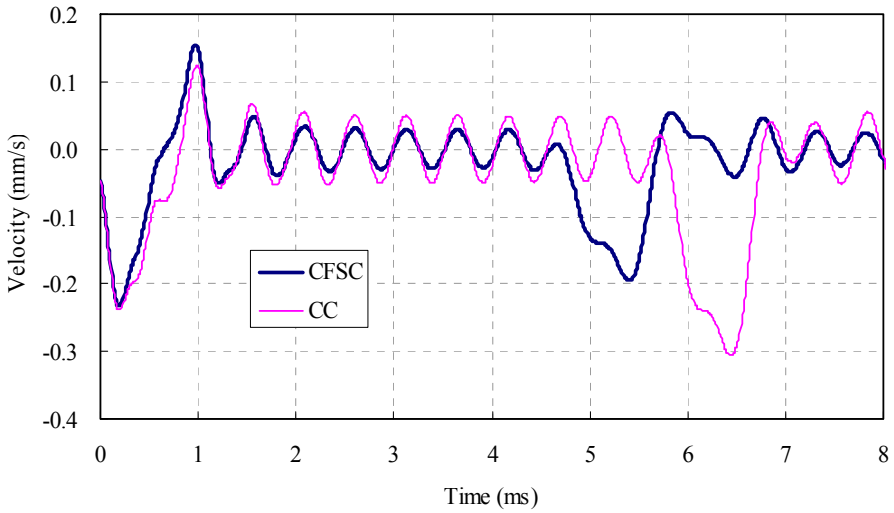

Fig. 10 Comparison of velocity responses of CFSC with CC at $r = 0.25R$

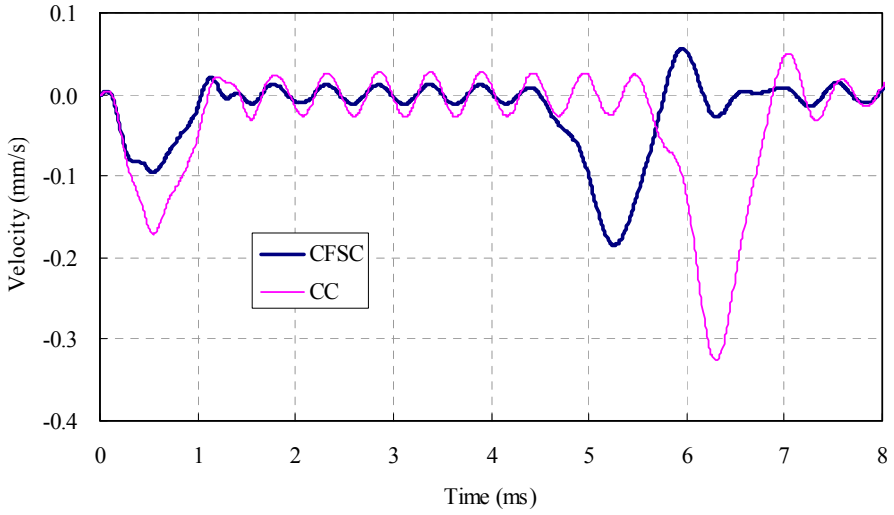

Fig. 11 Comparison of velocity responses of CFSC with CC at $r = 0.75R$

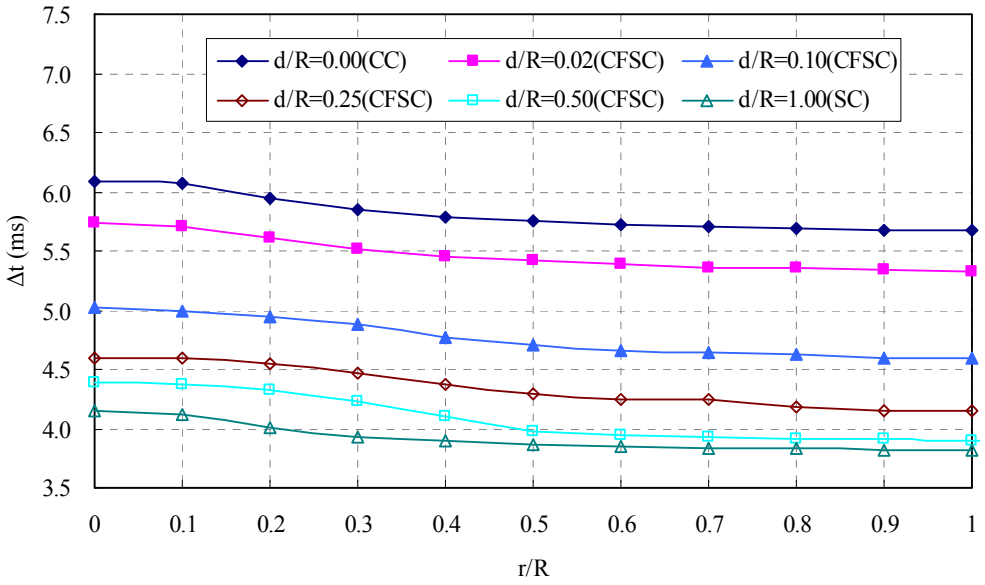

Fig. 12 Effects of d/R on time difference between incident and reflected wave peaks

are not the same. The results in Fig. 12 indicate that the time difference Δt is decreased with r/R. The time differences for these cases with different steel thickness have similar characteristics. The time difference varies significantly when $r/R < 0.6$, however, it is almost unchanged when $r/R \geq 0.6$.

Fig. 13 shows variation of time difference between incident and reflected wave peaks with d/R. The results reveal that a larger d/R results in a smaller Δt. The time differences decrease quickly with d/R when d/R is relatively small, however, they decrease slowly when d/R is relatively large and keep constant when $d/R \geq 0.8$.

Fig. 13 also presents the results calculated by 1D wave theory for reference. Based on 1D wave theory, the column is simplified as an one dimensional pole and the wave speed can be expressed as average speed of steel and concrete composite material as shown in Eq. (2).

$$C_{av} = \sqrt{\frac{m_s E_s + (1-m_s)E_c}{m_s \rho_s + (1-m_s)\rho_c}} \tag{2}$$

where m_s is the ratio of area of steel section to area of gross section; it can be calculated by $m_s = \left(2 - \frac{d}{R}\right)\frac{d}{R}$.

The results in Fig. 13 indicate that the time difference versus d/R calculated by 1D wave theory is close to the value calculated by 3D FEM when r/R is between 0.6 and 0.7. Therefore, when the accelerometer is placed between 0.6R and 0.7 R (about 2/3 R) in pulse-echo testing, the received velocity response will be close to the results predicted by 1D wave theory.

Fig. 14 shows effects of E_c on time difference between incident and reflected wave peaks. The wave speed decreases with the decrease of elastic modulus of the concrete as shown in Eq. (1),

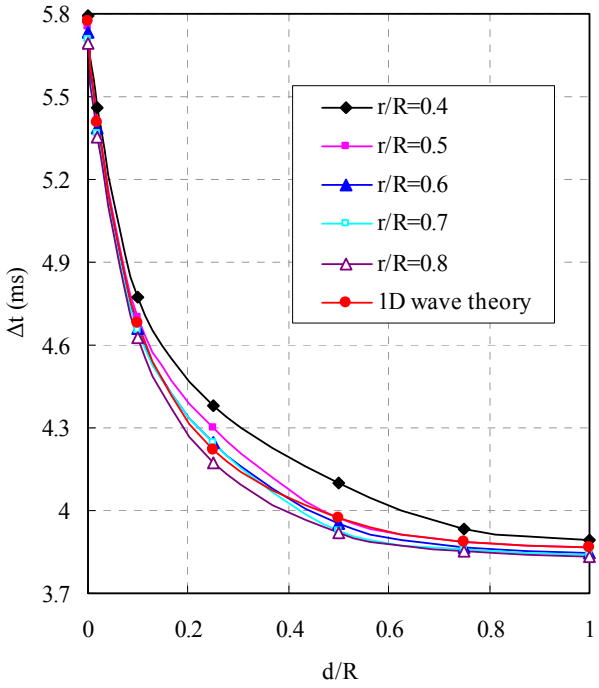

Fig. 13 Variation of time difference between incident and reflected wave peaks with d/R

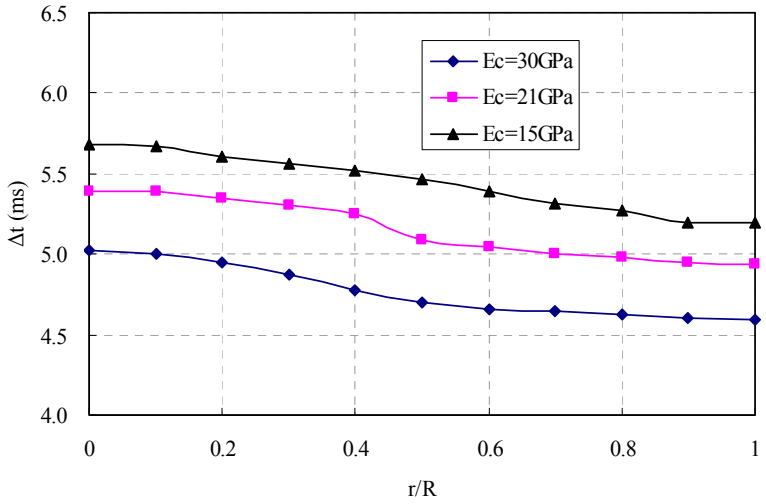

Fig. 14 Effects of E_c on time difference between incident and reflected wave peaks

therefore, the smaller elastic modulus results in larger time difference between incident and reflected wave peaks.

Fig. 15 shows the variation of time difference between incident and reflected wave peaks with R. The arrival time of the incident wave depends on the wave propagation distance. The larger the radius, the longer the distance from the center to the side of the column, therefore, the time

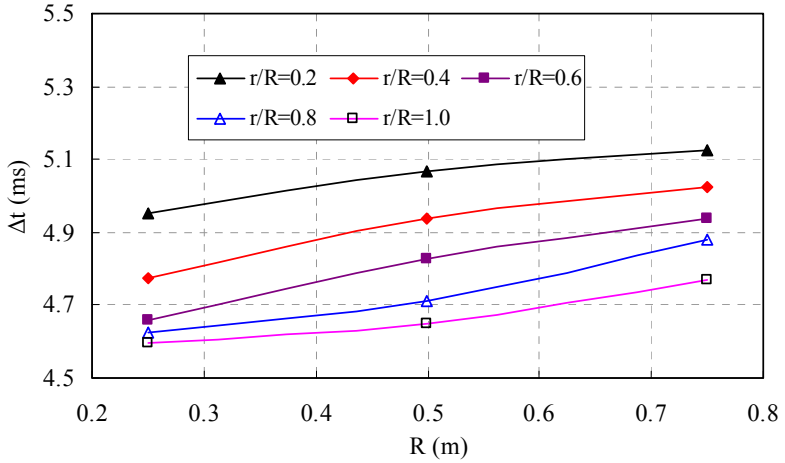

Fig. 15 Variation of time difference between incident and reflected wave peaks with R

difference is increased with R almost linearly.

5.3 Peak ratio of the incident and reflected waves

Fig. 16 shows effects of E_c on peak ratio of the incident and reflected waves, where v_i and v_r are peak values of incident and reflected waves, respectively. The peak value of the incident wave near the column center is the largest, therefore, the peak ratio of the incident and reflected waves is the largest at the location near column center (i.e., r/R = 0). The peak ratio decreases with r/R quickly when r/R is small, however, it almost keeps constant when r/R is large enough. The larger elastic modulus of the concrete causes smaller peak ratio when r/R is less than 0.6, however, the peak ratios corresponding to different E_c are almost the same when $r/R \geq 0.6$.

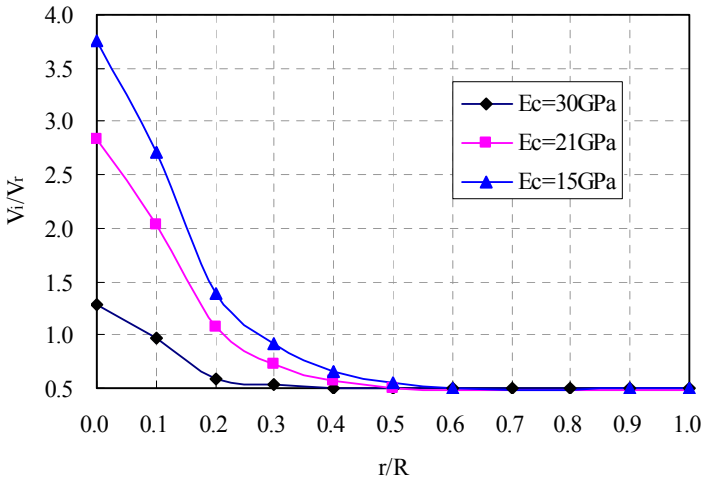

Fig. 16 Effects of E_c on peak ratio of the incident and reflected waves

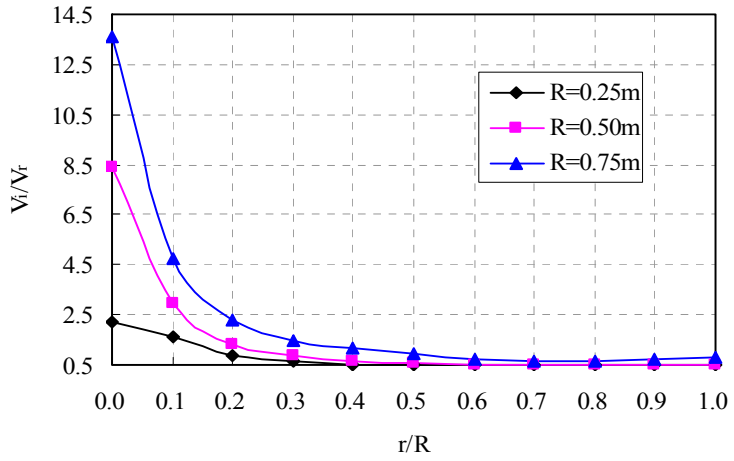

Fig. 17 Effects of R on peak ratio of the incident and reflected waves

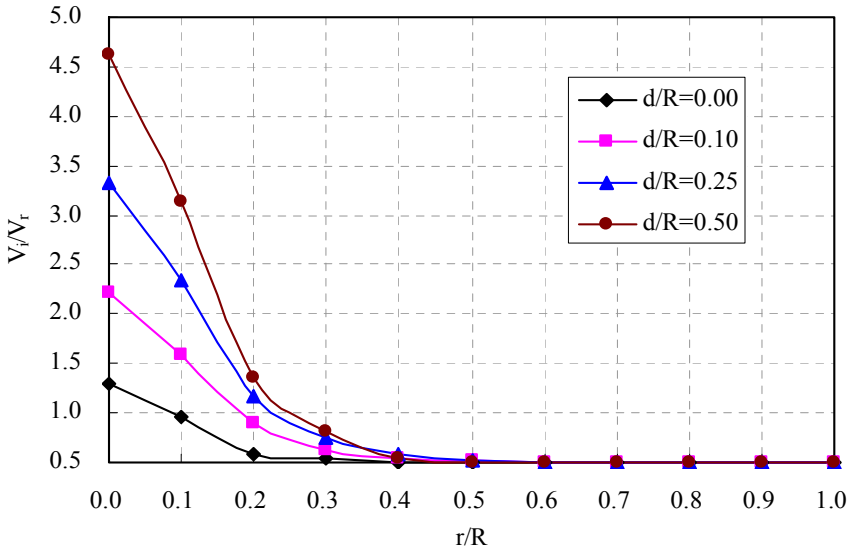

Fig. 18 Effects of d/R on peak ratio of the incident and reflected waves

The peak ratio of the incident and reflected waves is also influenced by radius R (as shown in Fig. 17). A larger radius results in a larger peak ratio. The peak ratios corresponding to R = 0.25 m, 0.5 m and 0.75 m when r/R = 0 are 2.4, 8.5 and 13.0, respectively. The differences among peak ratios with different R decrease quickly as the increase of r/R when it is less than 0.6 and then keep constant when it is greater than 0.6.

Fig. 18 shows effects of d/R on peak ratio of the incident and reflected waves. The peak ratios are affected by thickness of steel tube. The larger the thickness of steel tube (d/R), the larger the peak ratio of the incident and reflected waves. When r/R = 0 (at the column center), the peak ratios corresponding to d/R = 0.5, 0.25, 0.1 and 0 are 4.7, 3.3, 2.2 and 1.3, respectively. For the case of CC (d/R = 0), the peak ratio decreases with r/R obviously when $r/R \leq 0.4$, however, it almost

remains the same when $r/R > 0.4$. For the case of CFSC ($d/R > 0$), the peak ratios of the cases with different wall thickness of steel tube have little difference when $r/R > 0.6$.

The numerical results in Figs. 16 to 18 also reveal that the peak ratios of the incident and reflected waves are equal to 0.5 when r/R is large enough (i.e., $r/R > 0.6$), namely the peak value of reflected wave is double of the incident wave. Based on 1D wave theory for an elastic pole without any damping, the peak value of reflected wave from the column tip is double of the incident wave. Therefore, the peak ratio in this study shows good consistence with the results of 1D wave theory at the locations when $r > 0.6R$.

6. Conclusions

The wave propagation in CFSC due to transient impact load is studied by FEM. The propagation characteristics of the transient waves are analyzed in detail. The conclusions can be obtained as follows:

- The travel distance of the wave front in CFSC is farther than that in CC at the same time. For the different wave speed in steel and concrete, the wave front in CFSC presents an arch shape, the apex of which locates at the center of the column. The larger the radius, the higher the arch height. Differently, the wave front in CC presents a plane surface.
- Three dimensional effects and high-frequency waves are significant on the velocity response waveforms. The peak value and arrival time of the incident wave crests have great difference at different locations in the radial direction. Shorter distance to the column center results in larger peak value and earlier arrival time of incident waves. The high-frequency waves at the center and the side of CFSC have the largest phase difference and peak value.
- The time difference between incident and reflected wave peaks decreases with r/R significantly when $r/R < 0.6$, however, it almost keeps constant when $r/R \geq 0.6$. The time duration between incident and reflected waves calculated by 3D FEM is approximately equal to that calculated by 1D wave theory when r/R is about $2/3R$.
- The peak ratio of the incident and reflected waves is the largest at the location near the column center. The peak ratio decreases with r/R quickly when r/R is small, however, it almost keeps constant when r/R is large enough. The smaller concrete modulus, larger pile radius and steel tube thickness result in larger peak ratios when r/R is less than 0.6, however, the peak ratios are close to 0.5 when r/R is greater than 0.6.

Acknowledgments

The research described in this paper was financially supported by the National Natural Science Foundation of China (Grant No.51378177), the Program for New Century Excellent Talents in University (Grant No. NCET-12-0843), the Fundamental Research Funds for the Central Universities (Grant No. 106112014CDJZR200007) and the 111 project (Grant NO. B13024).

References

Alifujiang, X. and Akira, H. (2012), "Load-sharing ratio analysis of reinforced concrete filled tubular steel columns", *Steel Compos. Struct., Int. J.*, **12**(6), 253-540.

Bambach, M.R., Jama, H., Zhao, X.L. and Grzebieta, R.H. (2008), "Hollow and concrete filled steel hollow sections under transverse impact loads", *Eng. Struct.*, **30**(10), 2859-2870.
Chen, S.M. and Zhang, H.F. (2012), "Numerical analysis of the axially loaded concrete filled steel tube columns with debonding separation at the steel-concrete interface", *Steel Compos. Struct., Int. J.*, **13**(3), 277-293.
Chow, Y.K., Phoon, K.K., Chow, W.F. and Wong, K.Y. (2003), "Low strain integrity testing of pile: Three-dimensional effects", *J. Geotech. Geoenviron. Eng.*, **129**(11), 1057-1062.
Chung, K.S., Kim, J.H. and Yoo, J.H. (2013), "Experimental and analytical investigation of high-strength concrete-filled steel tube square columns subjected to flexural loading", *Steel Compos. Struct., Int. J.*, **14**(2), 131-153.
Ding, X.M., Liu, H.L., Liu, J.Y. and Chen, Y.M. (2011a), "Wave propagation in a pipe pile for low-strain integrity testing", *J. Eng. Mech. – ASCE*, **137**(09), 598-609.
Ding, X.M., Liu, H.L. and Zhang, B. (2011b), "High-frequency interference in low strain integrity testing of large-diameter pipe piles", *Sci. China – Technol. Sci.*, **54**(02), 420-430.
Ding, X.M., Liu, H.L. and Chen, Y.M. (2011c), "Analytical solution of wave propagation in large-diameter piles for low strain integrity testing", *Proceedings of the 2011 GeoHunan International Conference – Advances in Pile Foundations, Geosynthetics, Geoinvestigations, and Foundation Failure Analysis and Repairs*, Hunan, China, June, pp. 65-74.
Gajalakshmi, P. and Helena, H. (2012), "Behaviour of concrete-filled steel columns subjected to lateral cyclic loading", *J. Construct. Steel Res.*, **75**, 55-63.
Ge, H. and Usami, T. (1996), "Cyclic tests of concrete-filled steel box columns", *J. Struct. Eng., ASCE*, **122**(10), 1169-1177.
Huo, J., Zheng, Q., Chen, B. and Xiao, Y. (2009), "Tests on impact behaviour of micro-concrete-filled steel tubes at elevated temperatures up to 400 C", *Mater. Struct.*, **42**(10), 1325-1334.
Krause, M., Bärmann, M., Frielinghaus, R., Kretzschmar, F., Kroggel, O., Langenberg, K.J., Maierhofer, C., Müller, W., Neisecke, J., Schickert, M., Schmitz, V., Wiggenhauser, H. and Wollbold, F. (1997), "Comparison of pulse-echo methods for testing concrete", *NDT E International*, **30**(4), 195-204.
Mirmiran, A., Shao, Y.T. and Shahawy, M. (2002), "Analysis and field tests on the performance of composite tubes under pile driving impact", *Compos. Struct.*, **55**(2), 127-135.
Montejo, L.A., Gonzalez-Roman, L.A. and Kowalsky, M.J. (2012), "Seismic performance evaluation of reinforced concrete-filled steel tube pile/column bridge bents", *J. Earthq. Eng.*, **16**(3), 401-424.
Na, W.B. and Kundu, T. (2002), "EMAT-based inspection of concrete-filled steel pipes for internal voids and inclusions", *J. Pressure Vessel Tech. – Transact. ASME*, **124**(3), 265-272.
O'Shea, M. and Bridge, R. (2000), "Design of circular thin-walled concrete filled steel tubes", *J. Struct. Eng., ASCE*, **126**(11), 1295-1303.
Park, J.W. and Choi, S.M. (2013), "Structural behavior of CFRP strengthened concrete-filled steel tubes columns under axial compression loads", *Steel Compos. Struct., Int. J.*, **14**(5), 453-472.
Shan, J.H., Chen, R., Zhang, W.X., Xiao, Y., Yi, W.J. and Lu, F.Y. (2007), "Behavior of concrete filled tubes and confined concrete filled tubes under high speed impact", *Adv. Struct. Eng.*, **10**(2), 209-218.
Susantha, K., Ge, H. and Usami, T. (2002), "Cyclic analysis and capacity prediction of concrete-filled steel box columns", *Earthq. Eng. Struct. Dyn.*, **31**(2), 195-216.
Usami, T., Ge, H. and Saizuka, K. (1997), "Behaviour of partially concrete-filled steel bridge piers under cyclic and dynamic loading", *J. Construct. Steel Res.*, **41**(2-3), 121-136.
Wheeler, A. and Bridge, R. (2004), "The behaviour of circular conrete-filled thin-walled steel tubes in flexure", *Proceedings of the 5th International Conference on Composite Construction in Steel and Concrete*, Mpumalanga, South Africa, July.
Ye, W., Fan, Y.H., Zhao,W.g.G., Rong, Q. (2005), "Influence of the thickness of the steel tube on the length testing of the concrete-filled steel tube pile by means of stress wave", *J. Harbin Inst. of Technol.*, **37**(Supp2), 552-554.

CC